**HEFAT2011**
**8th International Conference on Heat Transfer, Fluid Mechanics and Thermodynamics**
**26 June – 1 July 2011**
**Pointe Aux Piments, Mauritius**

# EXPERIMENTAL STUDY ON CONDENSATION, FROST FORMATION AND CONDENSATE RETENTION ON MICROGROOVED AND PLAIN BRASS SURFACES UNDER NATURAL CONVECTION CONDITION

Rahman M. A.* and Jacobi A. M.
*Author for correspondence
Department of Mechanical Science and Engineering
University of Illinois at Urbana-Champaign,
Urbana 61801,
Illinois, USA,
E-mail: rahman5@illinois.edu

## ABSTRACT

In this study, frost was grown on microgrooved and baseline brass samples under specific operating conditions and a comparison of condensation, frosting and defrosting pattern on microgrooved and flat brass surfaces were carried out experimentally. The surfaces were fabricated by mechanical micro-machining process and no chemical alteration of the surface was conducted. It was found that the shape, size and distribution of condensed water droplets and subsequent frost structure are significantly affected by the micro-scale roughness on the surface. The condensed water droplets took an elongated shape and then coalesced along the pillars and grooves on grooved surfaces giving a parallel brick-like frosting pattern. The frost structure on the grooved surface was different than that on the flat surface and frost crystal exhibited more directional growth in the parallel to the surface direction, with numerous ice-flakes growing in the perpendicular and angular directions to the grooves. This non-uniform growth of the frost layer also gave the appearance of a spongy and loose frost structure and suggested the formation of less dense frost. Qualitative study of the spatial and temporal distribution of retained condensate on the grooved and plain brass surfaces after defrosting were carried out by analyzing thermal images of the sample surface during the defrosting period. Findings of this of this study can give significant insight about the frost properties and defrosting and condensate retention behaviour of heat transfer equipments with embedded microgrooves.

## INTRODUCTION

Frost formation on any solid surface, for example, the surface of a heat exchanger occurs when following two conditions are met – solid surface temperature is lower than dew point of the surrounding air and when it is also below the freezing point of water. Frost formation is usually considered to be undesirable in air conditioning, refrigeration and cryogenic equipments and systems because it causes an increase in pressure drop, reduction in air flow and overall decrease in heat transfer performance. Defrosting, which involves supplying heat to the surface of the heat exchanger to melt the frost and to remove it from the surface, then becomes necessary.

Frosting is undesirable for many reasons (all of which involves degradation of the heat exchanger performance and increase in operating cost) and therefore defrosting process is carried out which basically involves supplying heat to the heat transfer to melt the frost and to remove it from the surface. Defrosting has to be done in a periodic manner as some condensate retains on the surface after defrosting and frost forms again on the surface in the next heat transfer cycle. Very frequent defrosting is not desirable because not only the efficiency of the heat exchanger deteriorates, but also the overall operating cost increases due to the energy expenditure associated with the defrosting process.

Effect of surface wettability and micro-scale roughness on the condensation and frosting phenomenon has drawn considerable interest among the researchers [1-8]. Study of frost formation on a vertical or horizontal flat surface under natural convection conditions has been studied for a long time because of its obvious importance in numerous applications [9-13]. A number of works could be found in the open literature stressing the microscopic observation of frost formation pattern on hydrophobic or superhydrophobic surfaces fabricated either by chemically altering the surface roughness or by applying a coating over the surface [2-6]. The authors are unaware of any study of the effects of microscale surface roughness (produced by topographic modification) on the condensation, frosting and defrosting behaviour. The use of various techniques to create parallel grooves on aluminium surface by topographical modification without any chemical treatment was studied in these works [14-15] and very encouraging results on condensate drainage enhancement from these surfaces were reported. But they examined the drainage of condensed water droplets only; no test on the frosting/defrosting was reported by the authors of these papers.

Shin *et al.* [2] investigated the density and thermal conductivity variation of frost with the hydrophilicity of a surface. They found that frost formed on the surface with lower dynamic contact angle had higher thermal conductivity and density during the initial stages of the frosting test, but minor differences were observed after a longer frosting period (>2 hours). The effects of surface characteristics on the frosting/defrosting behaviour of an aluminium fin-tube heat exchanger were examined experimentally by Jhee *et al.* [6]. They found that frost of higher density grows on the hydrophilic surface and that of lower density grows on the hydrophobic surface compared to the bare aluminium heat exchanger. They argued that it was due to the difference in the droplet size and distribution density in the early frost growth period.

Narhe and Beysens [7-8] observed that condensed droplet on a hydrophobic or hydrophilic surface exhibits very different wetting characteristics from the behaviour observed for a placed or injected droplet. They investigated the wetting pattern and growth dynamics of condensed water droplets on a superhydrophobic surface with parallel microgrooves. They also identified different stages in the condensation process on the grooved surface and reported the growth pattern of the condensed droplets. The large condensed water droplets in the later part of the condensation process were found to be no longer in Cassie-Baxter wetting [16], but in Wenzel wetting regime [17].

Recently, Liu *et al.* [5] examined the frost deposition on a super-hydrophobic surface with micro-nano binary structure and observed chrysanthemum-like frost layer structure. They reported growth of the frost crystals along the parallel direction of the surface on the superhydrophobic surface instead of the normal vertical frost growth as observed on the plain copper surface.

In summary, although a significant amount of studies have been conducted on frost formation on vertical plate under natural convection and effects of surface treatment on frosting phenomenon, the authors are unaware of any work on the frost formation on microgrooved brass surface which are prepared by modifying the topographical features only. In the present study, condensation, frost formation and condensate retention pattern on microgrooved and flat brass surfaces have been investigated. Frost was grown on the samples under specific operating conditions inside a control chamber in natural convection. The difference in the condensation and frost formation pattern on the different surfaces were closely studied by visualizing the processes by a high speed camera equipped with microscopic zoom lens. The spatial and temporal distribution of condensate retention on the different surfaces after defrosting was examined by thermographic method. The thermal images were analyzed to identify the relative amount of different forms of retained condensate on the surfaces and the preliminary results are reported.

## EXPERIMENTS

In the present study, frosting/defrosting experiments were conducted on flat and microgrooved brass samples through

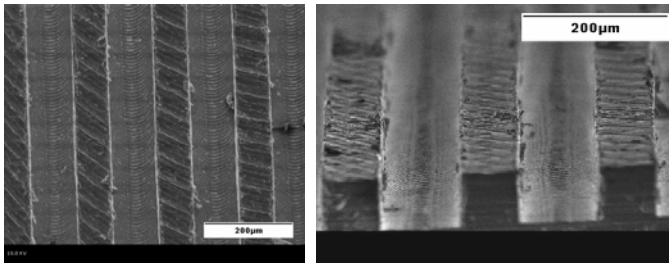


Figure 1 SEM images of the microgrooved sample. Machining burrs and marks can be seen on the groove and pillar surfaces

cooling the samples by a thermoelectric cooler. The microgrooved surfaces were fabricated by a mechanical micro-machining process known as micro end-milling using a Microlution 310-S machine. Brass alloy 360, an alloy mixture of copper and zinc was selected as the sample material for its very high machinability. End tools of 125 µm diameter were used to fabricate the sample used in the present study. Both the flat and microgrooved brass samples were 45 mm x 45 mm in size with a thickness of 3.175 mm. For inserting the thermocouple probes, 8 small holes of 2 mm diameter were drilled on the two sides of the sample plate. Scanning electron microscope (SEM) images of the microgrooved surfaces fabricated in this method are shown in Figure 1.

Static contact angle (SCA) was measured on these samples by sessile drop method using a CAM200 (KSV Instruments) optical goniometer. Measurements were taken at more than 6 different positions on each sample for a range of water droplet volumes. The microgrooved samples exhibited very high SCA in the direction parallel to grooves compared to that on the flat brass surface which was hydrophilic in nature (SCA≈ $68^0$). SCA on the microgrooved surface ranged from 132.67 to about $143^0$ in the parallel diction to the groove.

All the frosting/defrosting tests were carried out inside a thermally controlled chamber under specific operating conditions, in the presence of air at room temperature ($20\pm2^0$C). Schematic view of the experimental setup is shown in Figure 2**.** The test chamber was a rectangular box of plexi-glass and had a dimension of 12 x 12 x 8.5 $in^3$. There was a circular view- port at the front-side of the chamber to facilitate the test-time observation and recording of the frosting/defrosting process via a high speed camera (Phantom V60), equipped with a microscopic zoom lens. To measure the temperature of the sample during the tests, a total of eight thermocouples (E-type, measurement uncertainty of ± $0.13^0$C) were connected to the sample. Thermally conductive tape was used to attach samples to the thermo-electric cooler to ensure better contact.

A cool mist humidifier (Crane, EE-5301) was used to maintain the relative humidity (RH) inside the chamber at the desired value. Relative humidity level of air inside the chamber was measured by two capacitive hygrometers (accuracy ±2%), placed on the chamber wall on two sides of the sample. Both humidity and temperature measurement values were fed to a data acquisition system.

Before every frosting/defrosting test, the sample was properly cleaned by sonicating it in an acetone bath for 3-4

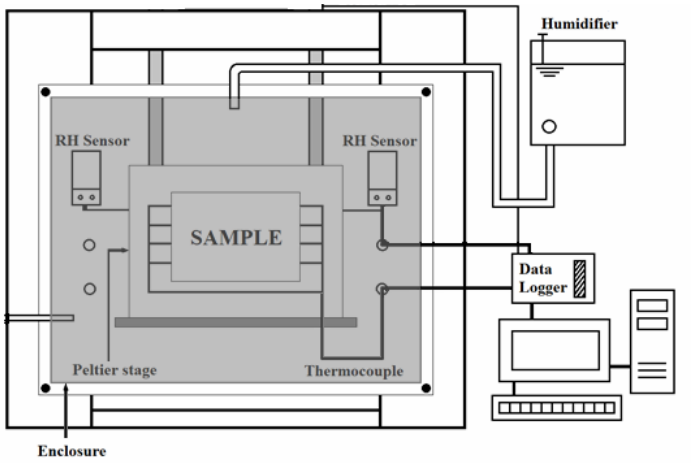

Figure 2 Schematic diagram of the experimental setup, showing different measurement devices and their connections

minutes, which was followed by rinsing with distilled water and isopropyl alcohol and was finally dried by compressed air flow. The Plate was then started to cool by switching the thermoelectric cooler on and setting the voltage of the DC power supply to the desired value. The frosting test was continued for 3 hours under specific relative humidity and plate temperature (-8 to -12$^0$C) conditions. The defrosting process was then carried out by either switching off the thermoelectric cooler or by supplying electric energy to the plate.

## RESULTS AND DISCUSSION

To ensure better comparison of the condensation, frost formation and defrosting process on the flat baseline and microgrooved brass samples, tests were conducted on a sample which had parallel microgrooves on its right half and plain surface on the other half. The plain portion of the surface was made flat and parallel by running a plaining operation with an end mill tool of 2.35 mm diameter. Frost was grown on the surface inside the thermally controlled chamber by cooling down the plate to temperatures of -8$^0$C to -12$^0$C under natural convection condition at relative humidity of 30 to 80%. Condensation, frost formation and defrosting pattern on these surfaces were observed and these processes were recorded via a high speed camera with a microscopic zoom lens. The flat brass surface was hydrophilic in nature with static contact angle of ≈ 68$^0$. On the other hand, the grooved portion of this surface had a static contact angle of ≈ 143$^0$ and 113$^0$ in the parallel and perpendicular direction to the groove respectively. Water drop placed on the grooved surface exhibited significant elongation in the direction of the grooves, due to the pinning of the three phase contact line by the groove edge.

### Condensation on Microgrooved and Flat Brass Surfaces

Figure 3 shows a series of successive pictures taken on the sample with both flat and microgrooved surfaces showing the growth, coalescence and merging of water droplets. A remarkable difference in the shape, size and distribution of water droplets on these two surfaces can be observed from these images. Nucleation of water droplets occurred at the same time on both the surfaces and very small droplets were

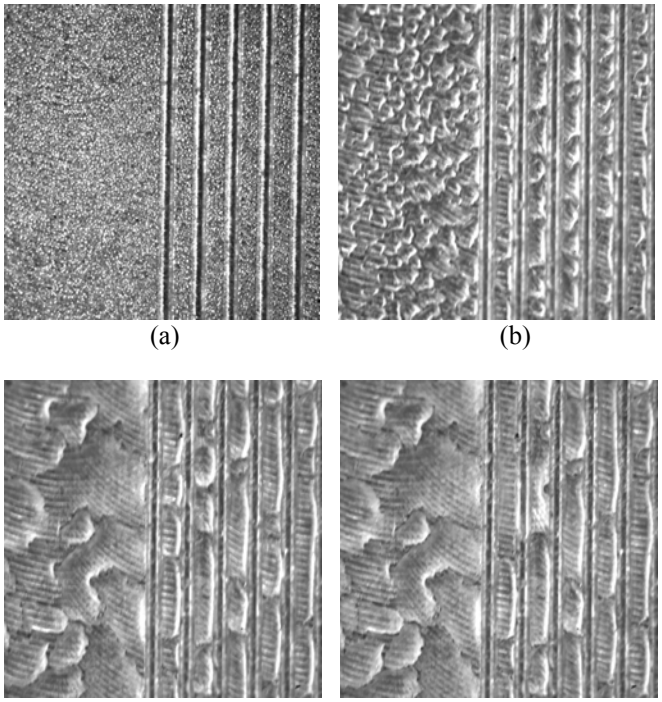

Figure 3 Growth, coalescence and merging of water droplets on flat baseline and microgrooved brass surface with increasing condensation under natural convection condition at a) 8 min b) 12 min c) 17 min and d) 17.30 min (just before freezing). A remarkable difference in the shape, size and distribution of water droplets on these two surfaces can be observed from these images

formed everywhere on the surface in the manner of dropwise condensation, as shown in Figure 3(a). At this stage of condensation, the droplets grew as individual, isolated droplets with a very small and equal average radius for both kinds of surfaces. However, with increasing condensation, droplets started to grow and merge with the adjacent water droplets to form bigger droplets. At this point, droplets on the flat baseline surface had an irregular, random shape and the droplets density on the surface (number of droplets on unit surface area) was higher than that on the microgrooved portion [Figure 3(b)]. The average size of the droplets on the flat surface was lower than that on grooved portion during this period. In the final stage of condensation, droplets on the flat surface started to merge together at a higher pace and formed very large droplets of random size and shape, covering most of the surface [Figures 3(c) and (d)]. The droplets coalesced in all directions and the drop size on the flat surface was few times greater than the droplets on the microgrooved portion.

On the other hand, the droplet growth pattern on the microgrooved surface during the condensation process was completely different. The drops formed on the pillars and grooved surfaces had an elongated shape in the direction of the grooves. Droplets on the pillars surface were found to grow at a higher rate and were typically bigger in size than droplets on the groove surface. During the initial stage of drop growth and merging, average size of the droplet on the grooved surface

(especially on the pillars) was higher than that on the baselines [Figure 3(b)]. The size of the droplets became larger as the droplets, both on the pillar and grooved surface, continued to grow and merging and coalescence of droplets occurred. As the condensation process continued, water droplets on the microgrooved surface were found to grow along the pillar and groove surfaces - assuming long, parallel-sided shape. This happened due to the well known pinning of droplets by the groove and pillar edges, which arrested the growth of the drop in the direction perpendicular to groove. It was observed that with increasing condensation, merging of the drops on the flat surface took place at a higher rate. Within few minutes, the size of the merged droplet on the baseline became bigger than the merged droplet on the grooved surface whose growth continued only in the parallel to groove direction. Water droplets on the pillar and groove surface had the length in the perpendicular to groove direction equal to the width of the pillars and grooves respectively.

The coalescence and merging of the drops on the groove surface occurred in a similar fashion as that on the pillars. As already mentioned, droplets were found to grow at a faster rate on the pillars than the grooves. This can be seen from form Figure 4(a), where although the droplets have already grown to considerably large size and covered almost the whole pillar surface, a significant portion of the groove surface was still not covered by the condensed water droplets. But as the condensation of vapour on the surface continued, droplets on the grooved surface grew and coalesced together to form a very long, column-like drop. The water droplets on two of the grooves are shown encircled by the yellow lines in Figure 4(a), which contained patches of dry portion between them**.** But from Figure 4(b) it can be seen that the water droplets on the grooves have merged together to form one very long chain of water drop covering the entire frame,

In our study, bridging between the droplets on the pillar and groove surface was not observed very frequently, unlike the study of Narhe and Beysens [7]. In most of the cases freezing of the droplets occurred before the droplets on either groove or pillar top became big enough to cause any bridging between them, either by rising or sinking of the droplets. But when it occurred, droplets on the groove and pillar merged together and formed a very large droplet covering 2-3 pillars on either side of the groove. This phenomenon can be observed more clearly from Figures 5(a) - (b**)** where by the bridging of water drops between two adjacent pillars and the grooves, single frozen droplet is seen to cover multiple pillars and grooves (encircled by red lines). From our experimental observations it was found that the frequency of occurrence of bridging of droplets sitting on the pillar and groove surfaces depends largely on the groove dimension and the cooling rate of the substrate. For the cases of higher groove depth and higher pillar width, the droplets on the pillars and groove do not merge together that frequently, even when the condensation process continues for a considerable amount of time. Also when the surface is cooled at a very high rate, freezing of the droplets takes place before the bridging of droplets between groove and pillars could occur.

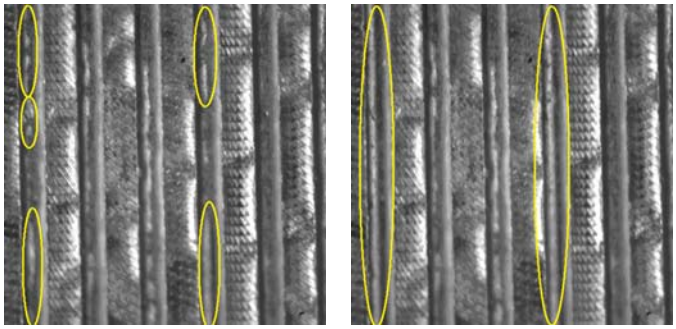

(a) (b)

Figure 4 Growth of condensed droplet on a microgrooved surface with groove height of 60 μm, groove width of 127 μm and pillar width of 190 μm. Droplets on the groove surface grew in size with time and then merged together to form a very long water drop as can be seen from (a) and (b)

**Frost Formation Pattern on the Microgrooved and Flat Brass Surfaces**

As cooling of the surface continued below the freezing point of water, freezing of the condensed droplets on both the plain and microgrooved surfaces occurred at the same time without any observable delay. Image of the droplets on both surfaces immediately after freezing are shown in Figure 5(a). The frosting test was continued up to 3 hours from the time of freezing of the water droplets on the surface. The structure and the pattern of the frost formation on both surfaces at different intervals of the test time are shown in Figures 5(b) - (h)**.**

After the freezing of the droplets, frost crystals started to grow in different directions on both surfaces in the same manner initially. Because of the difference in the droplet size, shape and orientation during the condensation stage, frozen droplets on the flat brass surface were very large in size and had small gaps of very thin film of frozen water between them. Frost crystal started to grow both on the thin layer and the big droplets, with small snow-flakes observable especially on the sides of the droplets [Figure 5(c)]. The **f**rost layer on the grooved surface, on the other hand, took the shape of a parallel 'brick-like' pattern, especially on the pillar surface as the elongated condensed water droplets on them froze. On the very few spots where bridging between droplets between groove and pillar surfaces occurred, the frozen droplet had relatively bigger size and the groove surface did not appear like a channel. Except that, the frost layer on the grooved surface was not easily observed and the grooves had the appearance of many dark channels in parallel.

The frost deposition on the surface continued with time and difference in the crystal growth pattern on the two surfaces became more evident. The frost crystals grew in a non-uniform manner in different directions on the grooved surface. This irregular growth of the frost layer can be seen from Figures 5(d)-(h). The frost crystals exhibited more directional growth in the parallel to the surface direction, with numerous ice-flakes growing in the perpendicular and angular directions to the grooves. This directional growth of the frost crystal gradually started to cover the empty surface over the grooves

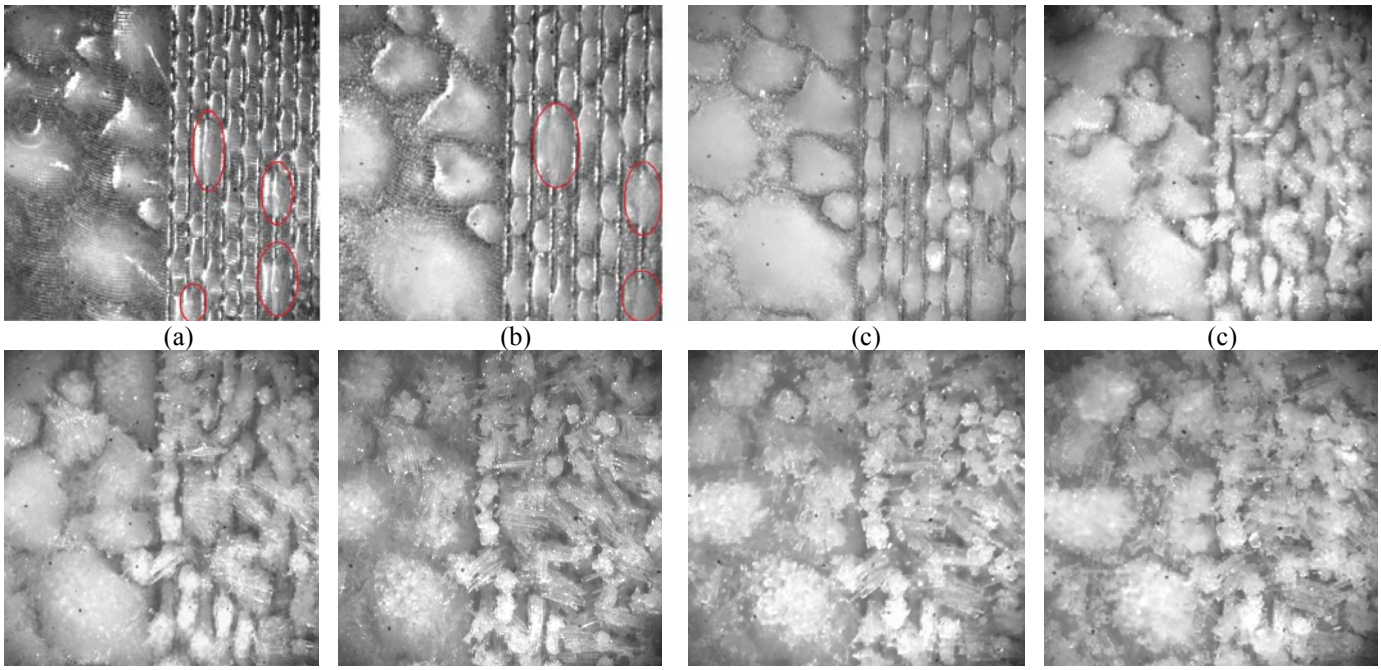

Figure 5 Frost formation pattern on the microgrooved and flat brass surfaces at different intervals of the frosting test. The difference in the frost formation pattern and structure on the two surfaces can be observed from these images taken at a) 48 min (immediately after freezing) b) 55 min c) 68 min d) 95 min e) 130 min f) 160 min g) 190 min h) 215 min. Frost was grown at a plate temperature of $-8^0$C and relative humidity of 30%.

and the parallel channels were no longer visible. This non-uniform and highly directional growth of the frost layer also gave the appearance of a spongy, loose frost structure and suggested the formation of less dense frost with plenty of voids in the frost structure. This also suggests highly irregular frost layer thickness on the microgrooved surface under this operating condition. The growth of the frost crystal on the plain surface, on the other hand, was found to be more in the normal to the surface direction. Frost layer growth was more uniform and had a denser looking frost structure on the plain surface. However, the difference in the frost pattern and structure became less distinguishable after very long frosting period, as can be seen in Figure 5(h), taken at the end of our 3 hour long frosting cycle

**l Distribution of Retained Condensate**

In most applications undergoing frosting/defrosting, the surface retains some of the frost melt water when it is defrosted for a specific period and this retained water readily freezes during the next frosting cycle. This retention of condensate at the end of defrosting process is usually an unavoidable, and at the same time, undesirable phenomenon. The spatial and temporal distribution of condensate retained on the surface after defrosting can serve as a very useful source of information for designing heat transfer surfaces with efficient condensate management. In this study, we tried to characterize the condensate retention pattern on the microgrooved and baseline brass surfaces by the method of thermal imaging. Images of the surfaces were taken at regular intervals during the defrosting period by an infrared camera (Brand: Mikron Midas, accuracy $\pm 2^0$C). The emissivity used for the surfaces was 0.3~0.5, which is the recommended emissivity for thermal imaging of burnished and oxidized brass surfaces. A series of thermal images on 1 baseline and 1 microgrooved sample at 4 different time periods (sample-1 with groove height ≈ 109 μm, groove width≈ 127 μm, pillar width ≈ 112 μm ) are shown in Figures 6 and 7**,** taken during the defrosting process after a frosting period of 3 hours. Defrosting process was carried out by supplying electric energy at a fixed rate for heating the substrate.

From careful experimental observation and also from the colour pattern of these IR images, the condensate on the surfaces was classified to be retained as one or more of the following 3 forms during different stages of defrosting – a) lump of water b) thick layer of water and/or as a c) thin film of water. At the later stages of defrosting, some parts of the surface started to get dry and this dry fraction of the surface increased as defrosting process was continued. These various forms of retained condensate had different colours (or range of colours) in the IR image due to their difference in temperature which could be easily distinguished and the knowledge of spatial distribution and relative amount of the different retained condensate forms could be gathered. Various forms of the retained condensate classified above are labelled in Figure 6.

From Figures 6 and 7 it can be seen that during the length of the defrosting process, big drops (lump) of water were retained mostly at the bottom of the sample surface, while a thick layer of water was retained on some parts of the surface

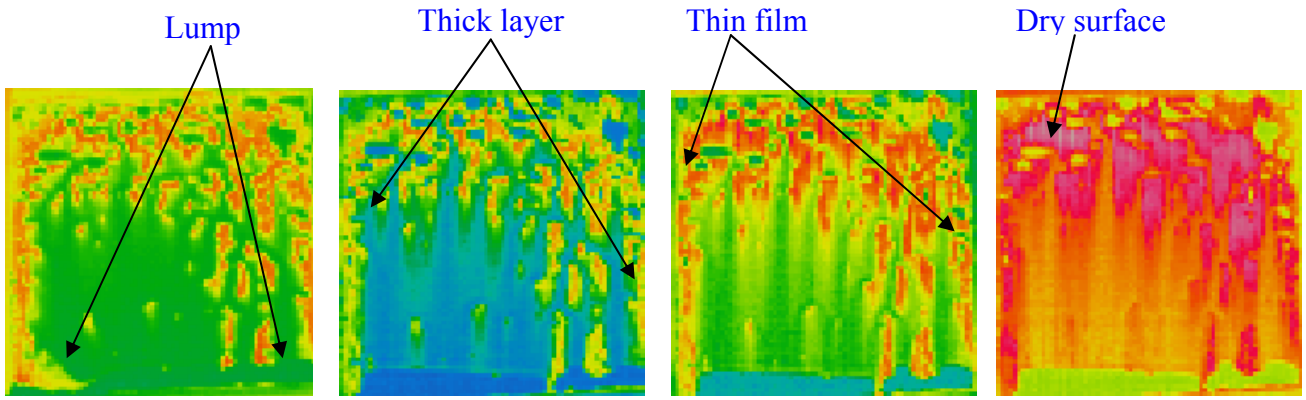

Figure 6 Thermographic images of baseline brass surface during different stages of defrosting process at a) 6 min b) 8 min c) 10 min d) 12 min. Based on the colour, different forms of retained condensate can be identified from the images.

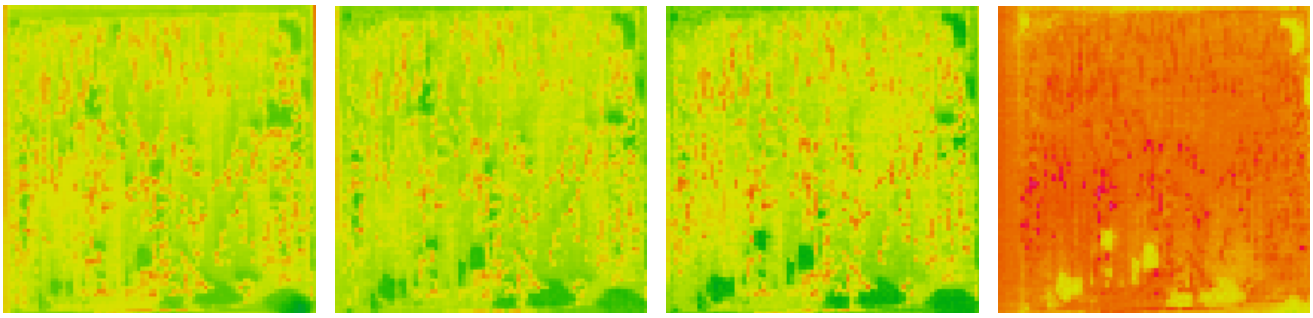

Fig. 7 Thermographic images of a microgrooved brass surface taken at a) 6 min b) 8 min c) 10 min and at d) 12 min of the defrosting process. Comparison of images of Figure 6 and Figure 7 reveals the difference in the water retention pattern between microgrooved and flat brass surfaces.

along with a very thin water film on some other parts. As time progressed, more condensate drained and the percentage of thick water layer retained on the surface started to reduce with the thick layer turning into thin condensate film. The bigger lump of retained condensate at the bottom was found to remain on the surface during the whole length of the defrosting process. With increasing time, both drainage and evaporation of condensate from the thin film occurred and the surface started to have few dry patches (shown in Figures 6(d) and 7(d)).

Comparison of Figures 6 and 7 enables us to qualitatively analyze the difference in water retention pattern on the flat baseline and the microgrooved surfaces. Both the spatial and time-wise distribution of condensate on the grooved surface was entirely different than the baseline. The baseline had more lumps of condensate during the initial stages of the defrosting process than the microgrooved surface [Figures 6(a), 6 (b) and 7(a)]. These lumps covered nearly the entire bottom-half of the sample till the 8$^{th}$ minute of defrosting. The flat baseline also retained more 'thick layer' form of condensate during most of the defrosting period. The grooved surface, on the other hand, had more 'thin film' of condensate retained on the surface, with small patches of 'thick layer' and 'lump' forms of condensate. This qualitative comparison thus also indicates lower condensate retention potential of the grooved surface at the end of defrosting period than flat baseline. At very later stages of the defrosting period, both the grooved and baseline surfaces exhibited small fraction of the surface which became dry [Figures 6 (d) and 7 (d)].

## CONCLUSION

Condensation, frost formation and condensate retention pattern after defrosting on microgrooved brass surface was observed to be significantly different than those on the flat brass surface. The microgrooved surfaces were fabricated by micro end-milling process and no chemical modification of the surface was implemented. First observable condensed water droplet on the surface was found to occur at the same time on both microgrooved and flat surfaces. Size, shape and distribution of condensed water droplets were found to vary considerably between the two surfaces. With increasing condensation, water droplet on the microgrooved surface assumed a long spherical shape along the grooves and pillars due to the pinning of droplets by the groove edges. Although the drop size was smaller on the flat surface in the earlier stages of condensation, the droplets merged and coalesced quickly with increasing condensation to form droplets bigger than that on the grooved surface. Bridging of condensed water droplet between adjacent grooves and pillars was found to be dependent on the cooling rate and dimension of the groove geometry. The frost structure on the grooved surface was different than that on the flat surface and the frost crystal exhibited more directional growth in the parallel to the surface direction. However, the difference in the frost pattern and structure became less distinguishable after very long frosting

period. Finally, qualitative study of the spatial and temporal distribution of retained condensate on the grooved and flat brass surfaces was carried out by means of thermal imaging.

## ACKNOWLEDGEMENT

We gratefully acknowledge the financial support from Air Conditioning and Refrigeration Centre (ACRC) at the University of Illinois at Urbana-Champaign.

## REFERENCES

[1] Hoke, J. L., Georgiadis, J. G., and Jacobi, A. M., 2000, The Interaction between the Substrate and Frost through Condensate Distribution,' *Technical report*, University of Illinois, Urbana-Champaign

[2] Shin J., Tikhonov A. V., Kim C., Experimental Study on Frost Structure on Surfaces with Different Hydrophilicity: Density and Thermal Conductivity, *Journal of Heat Transfer* 2003, Vol. 125 (85)

[3] Lee H., Shin J., Ha S., Choi B., Lee J., Frost formation on a plate with different surface hydrophilicity, *International Journal of Heat and Mass Transfer* 47 (2004) 4881–4893

[4] Liu Z.L., Zhang X.H., Wang H.Y., Meng S., Cheng S.Y., Influences of surface hydrophilicity on frost formation on a vertical cold plate under natural convection conditions, Exp. Therm. Fluid Sci. 31 (7) (2007) 789–794.

[5] Liu Z., Gou Y., Wang J., Cheng S., Frost formation on a super-hydrophobic surface under natural convection conditions, *International Journal of Heat and Mass Transfer*, 51 (2008) 5975–5982

[6] Jhee S., Lee K. S., Kim W. S., Effect of surface treatments on the frosting/defrosting behavior of a fin-tube heat exchanger *International Journal of Refrigeration* 25 (2002) 1047–1053

[7] Narhe R. D. and Beysens D. A., Nucleation and Growth on a Superhydrophobic Grooved Surface, *Physical Review Letters*, 2004, 93, 7

[8] Narhe R. D. and Beysens D. A., Growth Dynamics of Water Drops on a Square-Pattern Rough Hydrophobic Surface, *Langmuir* 2007, *23,* 6486-6489

[9] Hayashi Y., Aoki A., Adachi S., Hori K., Study of frost properties correlating with frost formation types, ASME J. Heat Transfer 99 (1977) 239–245.

[10] O'Neal D.L., Tree D.R., A review of frost formation in simple geometries, ASHRAE Trans. 91 (1985) 267–281

[11] Tao, Y. X., Besant, R. W., and Mao, Y., 1993, Characteristics of Frost Growth on a Flat Plate During the Early Growth Period, ASHRAE Trans., **99**, pp. 746–753.

[12] Fossa M., Tanda G., Study of free convection frost formation on a vertical plate, Experimental Thermal and Fluid Science 26 (2002) 661–668

[13] Hermes C.J.L., Piucco R.O., Barbosa Jr. J.R., Melo C., A study of frost growth and densification on flat surfaces, Experimental Thermal and Fluid Science 33 (2009) 371-379

[14] Sommers A. D., Jacobi A. M., Creating Micro-Scale Surface Topology to Achieve Anisotropic Wettability on an Aluminum Surface *J. Micromech. Microeng.* 2006, 16 1571–1578

[15] Liu L., Jacobi A. M., Chvedov D. 2009 A Surface Embossing Technique to Create Micro-grooves on an Aluminum Fin Stock for Drainage Enhancement, *J. Micromech. Microeng.* 19 (2009), pp. 35026-35034

[16] Cassie A. B. D. and Baxter S., Wettability of porous surfaces *Trans. Faraday Soc.*, 1944, 40, 546-551

[17] Wenzel, R. Resistance of Solid Surfaces to Wetting by Water *Ind. Eng. Chem.* 1936, *28*, 988